Met. Mater. Int., Vol. 22, No. 1 (2016), pp. 156~162
doi: 10.1007/s12540-015-5376-8

Hydrogen Gas Sensing of Co_3O_4-Decorated WO_3 Nanowires

Sunghoon Park[1], Gun-Joo Sun[1], Hyejoon Kheel[1], Soong Keun Hyun[1], Changhyun Jin[2], and Chongmu Lee[1,*]

[1]Department of Materials science and Engineering, Inha University, 253 Yonghyun-dong, Nam-gu, Incheon 402-751, Republic of Korea
[2]School of Mechanical Engineering, Konkuk University,120 Neungdong-ro, Gwangjin-gu, Seoul 143-701, Republic of Korea

(received date: 20 July 2015 / accepted date: 17 September 2015)

Co_3O_4 nanoparticle-decorated WO_3 nanowires were synthesized by the thermal oxidation of powders followed by a solvothermal process for Co_3O_4 decoration. The Co_3O_4 nanoparticle-decorated WO_3 nanowire sensor exhibited a stronger and faster electrical response to H_2 gas at 300 °C than the pristine WO_3 nanowire counterpart. The former showed faster response and recovery than the latter. The pristine and Co_3O_4-decorated WO_3 nanowire sensors showed the strongest response to H_2 gas at 225 and 200 °C, respectively. The Co_3O_4-decorated WO_3 nanowire sensor showed selectivity for H_2 gas over other reducing gases. The enhanced sensing performance of the Co_3O_4-decorated WO_3 nanowire sensor was explained by a combination of mechanisms: modulation of the depletion layer width forming at the Co_3O_4-WO_3 interface, modulation of the potential barrier height forming at the interface, high catalytic activity of Co_3O_4 for the oxidation of H_2, active adsorption of oxygen by the Co_3O_4 nanoparticle surface, and creation of more active adsorption sites by Co_3O_4 nanoparticles.

Keywords: oxides, Sol-gel, hydrogen, electrical conductivity/resistivity, gas sensor

1. INTRODUCTION

Hydrogen has many industrial applications such as fuel cells, hydrogen storage, hydrogen engine automobiles etc [1-3]. The development of high-performance hydrogen sensors is essential for human safety because hydrogen is flammable, explosive, invisible and odorless [4]. Gas chromatography or mass spectrometry systems have been employed for large-scale hydrogen sensing in industry, but they are unsuitable for many applications because they are heavy and expensive [5,6]. Therefore, the development of portable, cheaper and reliable hydrogen gas sensors is desirable.

Over the past few decades n-type metal oxide semiconductors such as SnO_2, ZnO, In_2O_3, and TiO_2 have been studied extensively as gas sensor materials [7-11], whereas fewer studies have evaluated p-type metal oxide semiconductors. This might be due to the inferior sensing properties of p-type metal oxide semiconductors from the viewpoint of sensing mechanism [12]. On the other hand, most of p-type metal oxide semiconductors have their own advantages for gas sensing such as strong catalytic activity for oxidation of reducing gas [13,14] and higher oxygen adsorption ability [15], i.e., higher solubility for oxygen compared to n-type metal oxide semiconductors, which can compensate for their inferior sensing properties. P-type metal oxide semiconductors with strong catalytic ability and high solubility of oxygen can be used effectively to produce high-performance gas sensors by being combined with n-type metal oxide semiconductors. Co_3O_4 is a typical p-type gas sensing material and has a strong catalytic activity for the oxidation of reducing gases.

On the other hand, tungsten oxide (WO_3) is an important n-type semiconducting material with a band gap of 2.7 eV, with applications, such as gas sensors, photocatalysts, and electrochromic devices [16]. Gas sensors based on WO_3 nanostructures have studied intensively owing to their excellent response and selectivity to various gases. WO_3 one-dimensional (1D) nanostructures is known to exhibit particularly strong responses to H_2 as well as NO_2, H_2S, O_3, NH_3, and liquefied petroleum gas at elevated temperatures (200-300 °C)[17-21]. Furthermore, the formation of p-n heterostructures enhances the sensing properties of WO_3 1D nanostructures. As is well known, WO_3 and Co_3O_4 are n- and p-type semiconductors, respectively.

This study examined the hydrogen sensing properties of Co_3O_4 nanoparticle-decorated WO_3 nanowires and the underlying mechanism for their enhanced sensing performance.

*Corresponding author: cmlee@inha.ac.kr

2. EXPERIMENTAL PROCEDURE

Co_3O_4 nanoparticle-decorated WO_3 nanowires were synthesized by the thermal evaporation of WO_3 powders in an oxidizing atmosphere, followed by spin-coating of the nanowires with Co_3O_4 nanoparticles and thermal annealing in an oxidizing atmosphere. First, Au-coated Si was used as the substrate for the synthesis of 1D WO_3 structures. A 3 nm-thick Au thin film was deposited on p-type (100) Si substrates by direct current (dc) magnetron sputtering. A quartz tube was mounted horizontally inside a tube furnace. 99.99% pure WO_3 powders were placed on the lower holder at the center of the quartz tube. The Au-coated Si substrate was placed on the upper holder, approximately 5 mm away from the WO_3 powders. The furnace was heated to 1,100 °C and maintained at that temperature for 1 h in a N_2/3mol%-O_2 atmosphere with constant flow rates of O_2 (10 standard cubic centimeter per minute (sccm)) and N_2 (300 sccm). The total pressure was set to 1.0 Torr.

In a separate step, a 100-mM Co_3O_4 precursor solution was prepared by dissolving cobalt acetate tetrahydrate ($Co(CH_3COO)_2 \cdot 4H_2O$) in distilled water. 40 ml of the Co_3O_4 precursor solution and 5 ml of 1-M NaOH solution were mixed together. This mixed solution was ultrasonicated for 30 min to form a uniform solution and then rotated using a centrifuge at 1,000 rpm for 2 min to precipitate the Co_3O_4 powders. The precipitated powders were collected by removing the liquid leaving the powders behind. The collected powders were rinsed in a 1:1:1-solution of acetone, isopropyl alcohol (IPA) and distilled water to remove the impurities. Subsequently, the Co_3O_4 precursor solution was dripped onto the WO_3 nanowires on a substrate and the substrate was rotated at 500 rpm for 30 s for Co_3O_4 decoration. After spin-coating, the Co_3O_4 decorated WO_3 nanowire sample was dried at 150 °C for 1 min and then annealed in air at 500 °C for 1 h.

The morphology and structure of the products were examined by scanning electron microscopy (SEM, Hitachi S-4200) operating at 10 kV and transmission electron microscopy (TEM, JEOL 2100F) with an accelerating voltage of 300 kV, respectively. The crystal structure of the nanowires was examined by 0.5° glancing angle X-ray diffraction (XRD, Philips X'pert MRD diffractometer) using Cu Kα radiation (λ = 0.15406 nm) at a scan rate of 4°/min.

Each nanowire sample was dispersed ultrasonically in a mixture of deionized water (5 m*l*) and isopropyl alcohol (5 m*l*). A 200-nm SiO_2 film was grown thermally on a single crystalline Si (100) substrate. A slurry droplet containing each nanowire sample (10 μ*l*) was dropped onto the SiO_2-coated Si substrates equipped with a pair of interdigitated (IDE) Ni (~200 nm)/Au (~50 nm) electrodes with a gap of 20 μm. The gas sensing tests were performed on the pristine WO_3 nanowire and Co_3O_4 nanoparticle-decorated WO_3 nanowire sensors at 200 °C in a quartz tube placed in a sealed chamber. The H_2 (> 99.99%) test gas was mixed with synthetic air to achieve the desired concentration. The H_2 gas flow rates were maintained at 200 cm^3/min using a mass flow controller to obtain H_2 concentrations of 50-2,000 ppm. A Keithley sourcemeter-2612 was used to acquire the resistance data. During the measurements, the sensors were placed in a sealed quartz tube with an electrical feed through. The electrical resistance of the nanowire sensor was monitored while a set amount of H_2 gas was injected into the testing tube. Details of the gas sensing test are described elsewhere [22].

3. RESULTS AND DISCUSSION

3.1. Structures of the pristine WO_3 and Co_3O_4 nanoparticle-decorated WO_3 nanowires

Figure 1(a) shows SEM image of the Co_3O_4 nanoparticle-decorated WO_3 nanowires synthesized in this study. The diameters of the WO_3 nanowires ranged from 60 to 300 nm and their length ranged up to a few hundreds of micrometers. The diameters of the Co_3O_4 particles were similar to those of the WO_3 nanowires, i.e., ranged from 50 to 300 nm (Inset in Fig. 1(a)). Figure 1(b) presents XRD patterns of the pristine WO_3 nanowires and Co_3O_4 nanoparticle-decorated WO_3 nanowires. All the XRD peaks in the pattern of the pristine WO_3 nanowires were assigned to orthorhombic WO_3 (JCPDS No. 89-4480, a = 0.739 nm, b = 0.757 nm, c = 0.779 nm). The XRD

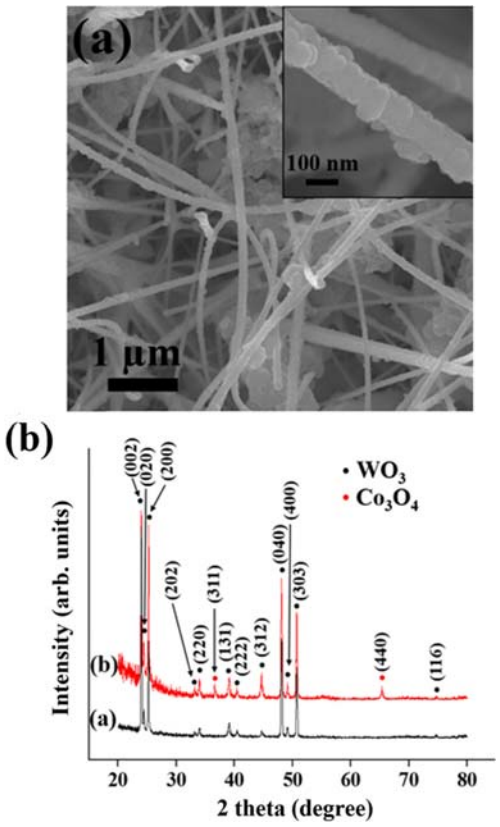

Fig. 1. (a) SEM image of the Co_3O_4-decorated WO_3 nanowires. (b) XRD patterns of the pristine and Co_3O_4-decorated WO_3 nanowires.

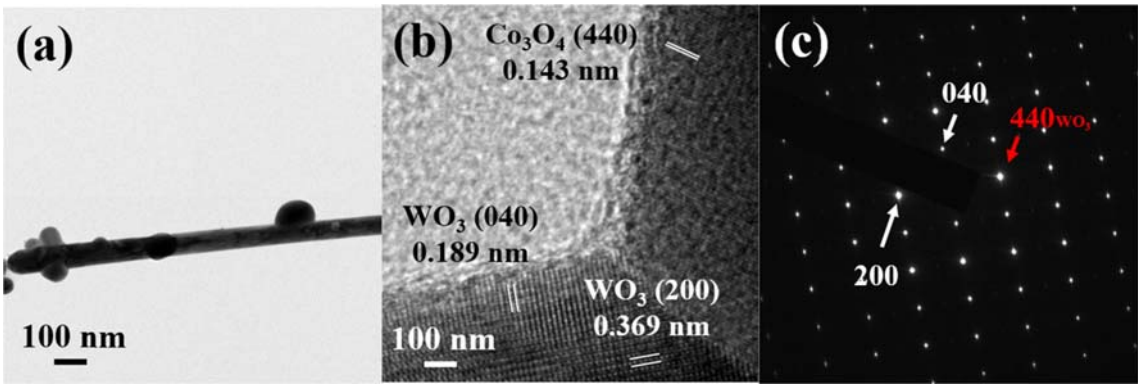

Fig. 2. (a) low-magnification TEM image, (b) HRTEM image, and (c) corresponding SAED pattern of Co_3O_4-decorated WO_3 nanowires.

pattern of the Co_3O_4 nanoparticle-decorated WO_3 nanowires exhibited a few peaks assigned to face-centered cubic-structured Co_3O_4 (JCPDS No. 78-1970, a = 0.809) in addition to those from WO_3, suggesting that the Co_3O_4 nanoparticles are polycrystalline. Figures 2(a)-(c) show a low-magnification TEM image, a high-resolution TEM (HRTEM) image and (c) corresponding selected area electron diffraction (SAED) pattern of Co_3O_4-decorated WO_3 nanowires. The Co_3O_4 nanoparticles showed a sphere-like morphology. The fringe pattern in the HRTEM image and the SAED pattern indicate the WO_3 nanowire to be a single crystal. In contrast, no clear fringe pattern is observable in the HRTEM image, but judging from the XRD pattern, HRTEM image and SAED pattern, Co_3O_4 nanoparticles might be polycrystalline.

3.2. Sensing performance of the pristine WO_3 nanowire and Co_3O_4 nanoparticle-decorated WO_3 nanowire sensors

Figures 3(a) and (b) show the transients of the pristine WO_3 nanowire and Co_3O_4 nanoparticle-decorated WO_3 nanowire sensors, respectively, at 200 °C to a typical reducing gas H_2. Upon exposure to H_2 gas, the resistance decreased rapidly and then increased slowly and subsequently recovered slowly to the initial value. The resistances showed good reversibility during the introduction and exhaust cycles of H_2 gas. Figure 3(c) shows the responses of the pristine WO_3 nanowire and Co_3O_4 nanoparticle-decorated WO_3 nanowire sensors as a function of the H_2 gas concentration. The response of the sensors is defined as R_a/R_g where R_a and R_g are the electrical resistances in the sensors in air and the target gas, respectively. The latter showed a stronger response with increasing H_2 concentration.

Figure 4(a) and (b) shows the response times and recovery times, respectively, of the pristine WO_3 nanowire and Co_3O_4 nanoparticle-decorated WO_3 nanowire sensors as a function of H_2 gas concentration. The response time and recovery time are defined as the times to reach 90% variation in resistance upon exposure to H_2 and air, respectively. Both the Co_3O_4 nanoparticle-decorated WO_3 nanowire sensor showed shorter response and recovery times than the pristine WO_3 nanow-

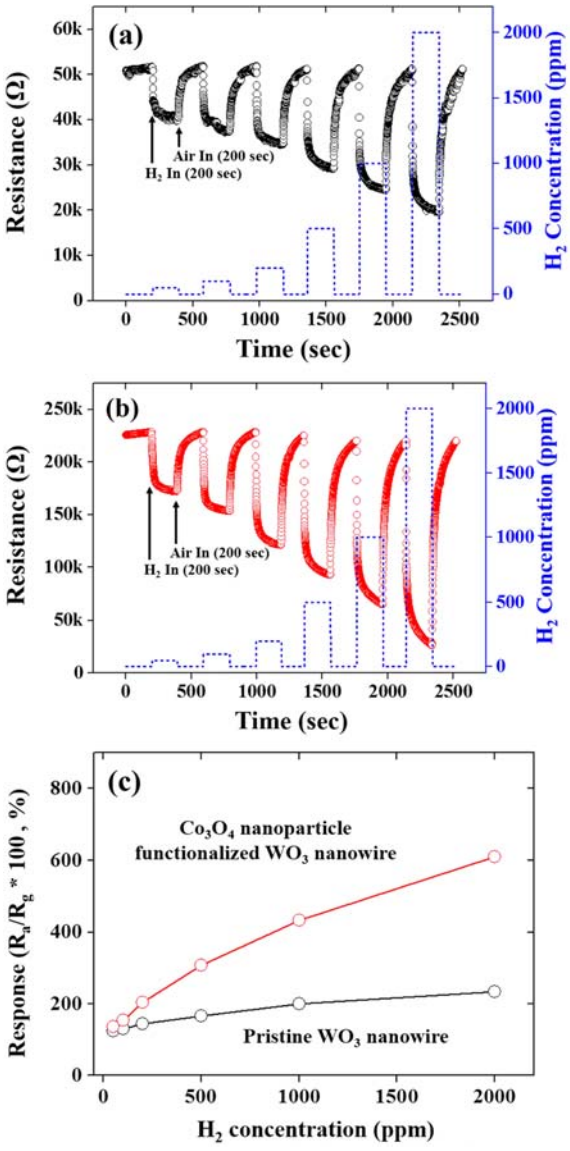

Fig. 3. Gas sensing transients of (a) the pristine WO_3 nanowire sensor and (b) Co_3O_4-decorated WO_3 nanowire sensor to 50, 100, 200, 500, 1,000 and 2,000 ppm H_2 gas at 200 °C. (c) Responses of the pristine WO_3 nanowire sensor and Co_3O_4-decorated WO_3 nanowire sensor as a function of the H_2 gas concentration at 200 °C.

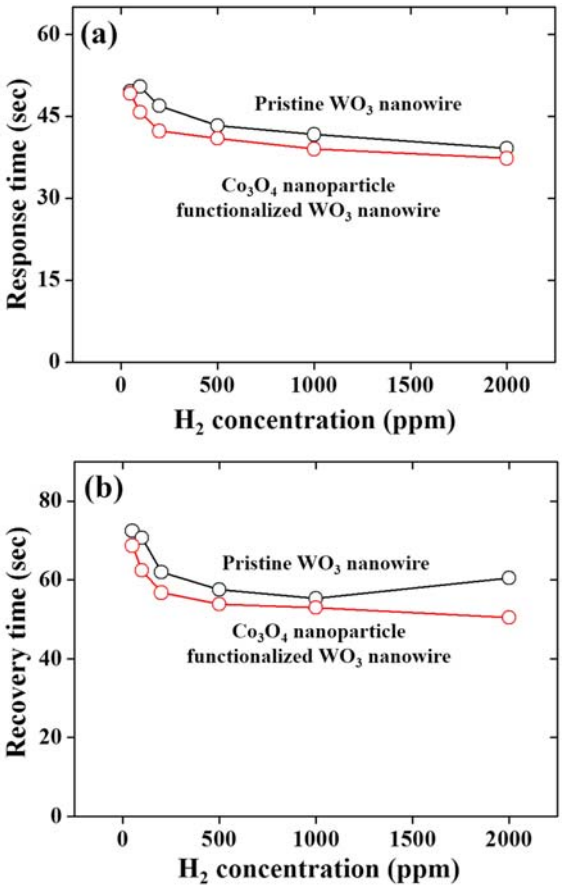

Fig. 4. (a) Response times and (b) recovery times of the pristine and Co_3O_4-decorated WO_3 nanowire sensors as a function of H_2 gas concentration at 200 °C.

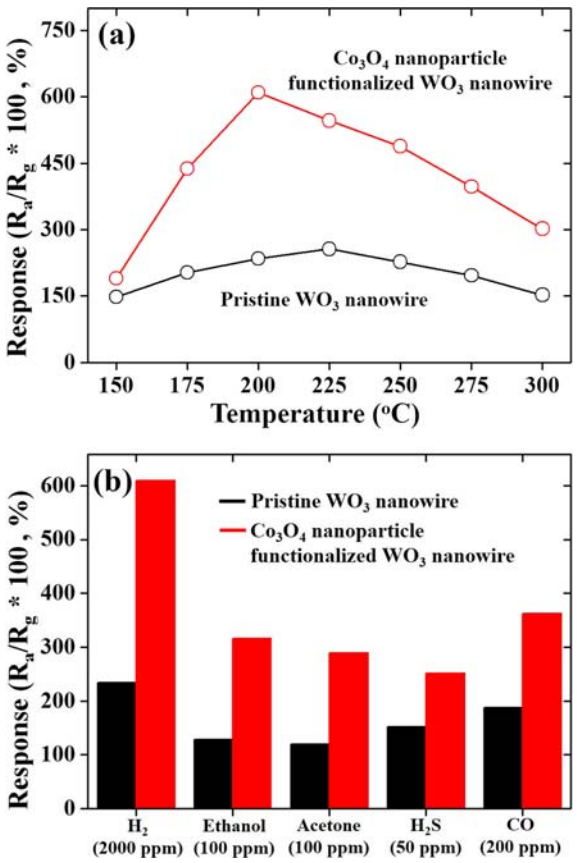

Fig. 5. (a) Responses of the pristine and Co_3O_4-decorated WO_3 nanowire sensors as a function of the operation temperature. (b) Responses of the pristine and Co_3O_4-decorated WO_3 nanowire sensors to various gases.

ire sensor, but the difference was small. The response and recovery times as well as the response of a sensor material to a certain gas might also depend on a range of factors such as the solid solubility of the gas in the material, decomposition rate of the adsorbed molecule at material surface, charge carrier concentration in the material, Debye length in the material, catalytic activity of the material, and orbital energy of the gas molecule. On the other hand, the results in this study show strong dependence of the response but weak dependence of the response time and recovery time on those factors. This difference is not completely understood, but it might be caused by the large activation energies for the adsorption of O_2 and H_2 and the decomposition of H_2. The response time and recovery time depend strongly on the activation energies of the related reactions, whereas the response does not [23].

The responses of the pristine WO_3 nanowire and Co_3O_4 nanoparticle-decorated WO_3 nanowire sensors to H_2 gas were plotted as a function of the operation temperature as shown in Fig. 5(a). The pristine WO_3 nanowire and Co_3O_4 nanoparticle-decorated WO_3 nanowire sensors showed a maximum response at 225 °C and 200 °C, despite the small differences in response between 200 °C and other temperatures in the case of the former. In contrast, the Co_3O_4 nanoparticle-decorated WO_3 nanowire sensor showed the strongest response at 200 °C. These results indicate the optimal operation temperatures for the pristine WO_3 nanowire and Co_3O_4 nanoparticle-decorated WO_3 nanowire sensors are 225 °C and 200 °C, respectively and that the optimum operation temperature of the latter is 25 °C lower than that of the former. Based on these results, all other sensing tests were carried out at 200 °C. At low temperatures, upon exposure to oxygen, because of the inactive ionosorption of oxygen due to the few active adsorption sites at the WO_3 and Co_3O_4 surfaces, inactive oxidation of hydrogen gas occurs, resulting in poor response. Vacancies and kink sites at the surface of a material are preferential sites for the adsorption of impurity atoms or ions. At low temperatures the surface contains lower concentrations of vacancies and kink sites, resulting in the inactive oxidation of hydrogen gas and a poor response.

As the operating temperature increases, the adsorption of oxygen on the sensor surface becomes active, and oxidation of H_2 becomes more active, resulting in an enhanced response to H_2 gas. On the other hand, further increases in tempera-

ture than the optimal temperature will result in desorption of species [24]. The decrease in the optimal operation temperature of WO_3 nanowires by Co_3O_4 particle-decoration might be due to the easier desorption of species at the surface in the Co_3O_4 particle-decorated WO_3 nanowires than the pristine WO_3 nanowires. Co_3O_4 might possess catalytic activity that promotes the desorption of species from the surface as well as the oxidation of H_2. Therefore, the desorption of species begins to occur at a lower temperature in the Co_3O_4 particle-decorated WO_3 nanowires than in the pristine WO_3 nanowires.

Figure 5(b) shows the selectivity of the pristine WO_3 nanowire and Co_3O_4 nanoparticle-decorated WO_3 nanowire sensors for H_2 gas over other reducing gases including H_2. The responses to these gases were measured at 200 °C. Different concentrations were chosen for different gases considering the minimum concentration of each gas allowed from the viewpoint of human safety. Both the pristine WO_3 nanowire and Co_3O_4 nanoparticle-decorated WO_3 nanowire sensors showed selectivity to H_2 gas over the other gases tested. In particular, the Co_3O_4 nanoparticle-decorated WO_3 nanowire sensor showed higher selectivity than the pristine nanostructure sensor. The reason for why the response of the Co_3O_4-decorated WO_3 nanowires to H_2 at 200 °C was higher than those to other gases is not completely understood at the present. One possible reason is that Co_3O_4 possesses electrocatalytic properties of enhancing H_2 oxidation. The H_2 oxidation reaction will be enhanced by Co_3O_4, resulting in a more significant increase in electron concentration and a larger decrease in resistance in the WO_3 nanowire sensor than other material sensors. Another reason might be related to the different optimal operating temperatures of the sensor for different target gases. The response of a sensor material to a certain gas might depend on a range of factors such as the solid solubility of the gas in the material, decomposition rate of the adsorbed molecule at the material surface, charge carrier concentration in the material, Debye length in the material, catalytic activity of the material, orbital energy of the gas molecule, etc. The oxidation rate of a gas is determined by these factors. Therefore, each gas has the characteristic optimal oxidation temperature at which its oxidation rate is maximized. The Co_3O_4–decorated WO_3 nanowire sensor fabricated in this study showed stronger response to H_2 than other gases at 200 °C because of the higher oxidation rate of H_2 at the surface of Co_3O_4 and WO_3 at that temperature, but the sensor might show stronger responses to other gases, such as ethanol at different temperatures [23].

3.3. Sensing mechanism of the Co_3O_4 nanoparticle-decorated WO_3 nanowire sensor

The hydrogen sensing mechanism of metal oxide semiconductors is well established based on the surface depletion model and can be summarized as follows [25,26]:

In air, oxygen molecules are chemsorbed on the WO_3 nanowire surface and form oxygen ions by extracting electrons from the conduction band of WO_3 [27,28]:

$$O_2(g) = O_2(ad) \quad (1)$$
$$O_2(ad) + e^- = O_2^-(ad) \quad (2)$$
$$O_2^-(ad) + e^- = 2O^-(ad) \quad (3)$$

These reactions produce an electron depletion region near the WO_3 nanowire surface, leading to an increase in resistance. If the nanowire sensor is exposed to hydrogen gas, the hydrogen molecules will react with the adsorbed oxygen species [29].

$$H_2 + 1/2\ O_2^-(ad) = H_2O + e^- \quad (4)$$
$$H_2 + O^-(ad) = H_2O + e^- \quad (5)$$

These reactions are exothermic and the H_2O molecules produced will desorb from the surface. The electrons released will decrease the depletion layer width, leading to a decrease in the resistance of the nanowire sensor. Upon exposure of the sensor to the air ambient, the depletion layer width will increase again by adsorbing oxygen species as expressed in Eqs. (1)-(3). The resistance will recover to its initial level. The surface chemisorption of dissociated hydrogen might play an important role in hydrogen sensing. During chemisorption hydrogen dissociated on the surface of a semiconductor acts as a surface state and electron transfer takes place from hydrogen to the conduction band of WO_3. This results in the formation of an electron accumulation layer on the WO_3 nanowire surface, leading to a decrease in resistance. If the hydrogen gas supply is stopped, electron transfer back to hydrogen will occur, resulting in recovery of the original resistance due to the elimination of the accumulation layer.

The enhanced response of the Co_3O_4-decorated WO_3 nanowire sensor can be explained by a combination of the following factors: (1) modulation of the depletion layer width forming at the Co_3O_4-WO_3 interface, (2) modulation of the potential barrier height forming at the interface, (3) the high catalytic activity of Co_3O_4 for the oxidation of H_2, (4) active adsorption of oxygen by the Co_3O_4 nanoparticle surface and (5) creation of more active adsorption sites by Co_3O_4 nanoparticles. First, upon exposure to air a depletion layer forms on the Co_3O_4 side and an accumulation layer forms on the WO_3 side of the p-Co_3O_4/n-WO_3 interface. Upon exposure to H_2 gas a reverse situation occurs, i.e., depletion layers form on both the Co_3O_4 and WO_3 sides. Therefore, modulation of the depletion layer occurs due to the difference in the depletion layer width ($L_D(WO_3)$ - $L_D(Co_3O_4)$) formed at the interface between in air and in H_2 gas (Fig. 6). Second, one of the important differences between the pristine and Co_3O_4-decorated WO_3 nanowire sensor is the existence of p-n heterojunctions in the latter. A potential barrier forms at the Co_3O_4/WO_3 p-n junction and potential barrier height modulation occurs during the adsorption and desorption of H_2 gas [30,31]. The difference in potential barrier height at the p-n junction is V_2-V_1

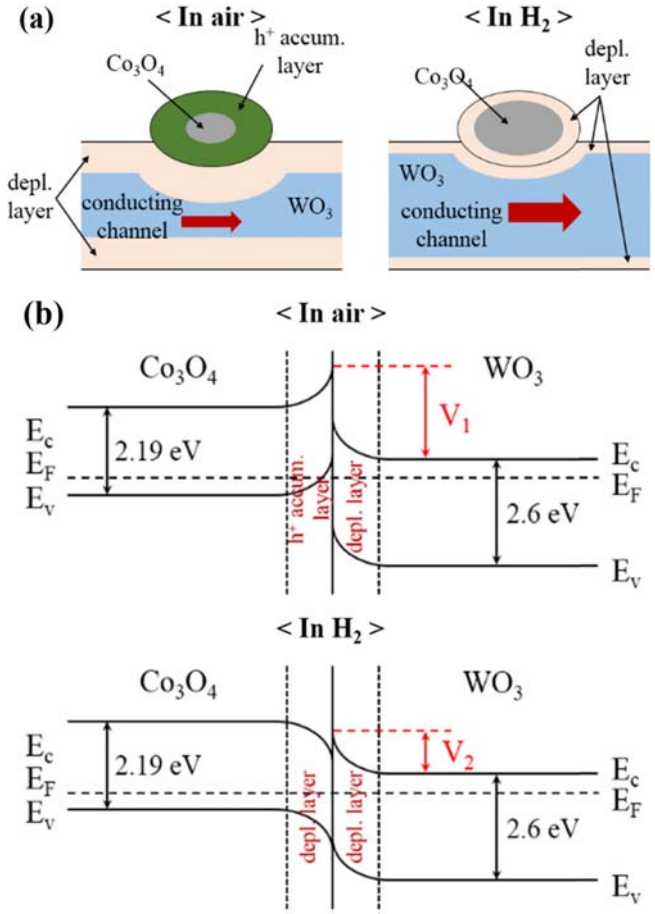

Fig. 6. Energy band diagram of the Co_3O_4-WO_3 system in air and H_2 gas: bandgap of WO_3 = 2.6 eV [31], bandgap of Co_3O_4 = 2.19 eV [32].

between in air and in H_2 gas as shown in Fig. 5 [32-33].

The resistance of the sensor is related to the potential barrier height by the following Eq. [34]:

$$R = R_0 \exp(qV/kT) \quad (6)$$

where R is the resistance of the material, R_0 is the initial resistance, q is the charge of an electron, V is the potential energy barrier height, k is Boltzmann's constant, and T is the temperature of the sensing material. Because the response is determined by R_a/R_g, the response depends on the potential barrier at the Co_3O_4/WO_3 interface. Third, the oxidative catalytic activity of cobalt oxide is relatively well-known [35-39]. Co_3O_4 plays the role of a catalyst to expedite the oxidation reaction of hydrogen, leading to enhanced response to H_2 gas. Fourthly, most p-type oxide semiconductors adsorb oxygen actively. The distinctive oxygen adsorption of Co_3O_4 might also contribute to an enhancement of the response of the Co_3O_4 nanoparticle-decorated WO_3 nanowire sensor to H_2 gas. The active adsorption of oxygen by the Co_3O_4 surface would consume more electrons and thereby produce a thicker electron depletion layer, which, in turn, would result in a further increase in electrical resistance. On the other hand, the response is determined by R_a/R_g where R_a and R_g are the electrical resistances in the sensors in air and the target gas, respectively. Assuming that this remains the same, an increase in electrical resistance would lead to stronger response. Lastly, the lattice mismatch between Co_3O_4 and WO_3 generates structural defects at the Co_3O_4-WO_3 interface, which acts preferential adsorption sites for hydrogen and oxygen molecules.

4. CONCLUSIONS

The multiple networked Co_3O_4-decorated WO_3 nanowire sensor showed enhanced electrical responses to H_2 gas at 200 °C compared to the pristine WO_3 counterpart. The pristine and Co_3O_4-decorated WO_3 nanowires exhibited responses of 234% and 610%, respectively, to 2,000 ppm H_2 at 200 °C. The enhanced response of the Co_3O_4-decorated WO_3 nanowire sensor can be explained by a combination of the following factors: modulation of the depletion layer width and potential barrier height forming at the Co_3O_4-WO_3 interface, high catalytic activity of Co_3O_4 for the oxidation of H_2, active adsorption of oxygen by the Co_3O_4 nanoparticle surface, and the creation of more active adsorption sites by Co_3O_4 nanoparticles. The optimal operation temperatures of the pristine and Co_3O_4 were determined.

ACKNOWLEDGMENTS

This study was supported by the Basic Science Research Program through the National Research Foundation of Korea (NRF) funded by the Ministry of Education (2010-0020163).

REFERENCES

1. J. Tamaki, T. Maekawa, N. Miura, and N. Yamazoe, *Sensor. Actuat. B-Chem.* **9**, 197 (1992).
2. T. Hübert, L. Boon-Brett, G. Black, and U. Banach, *Sensor. Actuat. B-Chem.* **157**, 329 (2011).
3. L. Fields, J. Zheng, Y. Cheng, and P. Xiong, *Appl. Phys. Lett.* **88**, 232 (2006).
4. K. Skucha, Z. Fan, K. Jeon, A. Javey, and B. Boser, *Sensor. Actuat. B-Chem.* **145**, 232 (2010).
5. M. Ramanathan, G. Skudlarek, H. H. Wang, and S. B. Darling, *Nanotechnology* **21**, 125501 (2010).
6. K. J. Liekus, I. A. Zlochower, K. L. Cashdollar, S. M. Djordjevic, and C. A. Loehr, *J. Loss Prevent. Proc.* **13**, 377 (2000).
7. S. Park, S. An, H. Ko, C. Jin, and C. Lee, *ACS Appl. Mater. Interfaces* **4**, 3650 (2012).
8. Y. J. Kwon, H. G. Na, S. S. Kim, P. Wu, and H. W. Kim, *Met. Mater. Int.* **21**, 956 (2015).
9. J. H. Yoon and J. S. Kim, *Met. Mater. Int.* **16**, 773 (2010).
10. J. M. Lim, K. C. Shin, H. W. Kim, and C. Lee, *Thin Solid Films* **475**, 256 (2005).

11. M. Law, H. Kind, B. Messer, F. Kim, and P. Yang, *Angew. Chem. Int. Edit.* **41**, 2511 (2002).
12. W. Zheng, X. Lu, W. Wang, Z. Li, H. Zhang, Y. Wang, Z. Wang, and C. Wang, *Sensor. Actuat. B-Chem.* **142**, 61 (2009).
13. S. Park, S. An, Y. Mun, and C. Lee, *ACS Appl. Mater. Interfaces* **5**, 4285 (2013).
14. A. S. Zoolfakar, M. Z. Ahmad, R. A. Rani, J. Z. Ou, S. Balendhran, S. Zhuiykov, K. Latham, W. Wlodarski, and K. Kalantar-zadeh, *Sensor. Actuat. B-Chem.* **185**, 620 (2013).
15. K. Pirkanniemi and M. Sillanpää, *Chemosphere* **48**, 1047 (2002).
16. M. M. Bettahar, G. Costentin, L. Savary, and J. C. Lavalley, *Appl. Catal. A-Gen.* **145**, 1 (1996).
17. H. R. Kim, K. I. Choi, K. M. Kim, I. D. Kim, G. Cao, and J. H. Lee, *Chem. Commun.* **46**, 5061 (2010).
18. H. T. Sun, C. Cantalini, L. Lozzi, M. Passacantando, S. Santucci, and M. Pelino, *Thin Solid Films* **287**, 258 (1996).
19. B. Cao, J. Chen, X. Tang, and W. Zhou, *J. Mater. Chem.* **19**, 2323 (2009).
20. A. Ponzoni, E. Comini, G. Sberveglieri, J. Zhou, S. Z. Deng, N. S. Xu, Y. Ding, and Z. L. Wang, *Appl. Phys. Lett.* **88**, 203101 (2006).
21. O. Merdrignac-Conanec and P. T. Moseley, *J. Mater. Chem.* **12**, 1779 (2002).
22. J. H. Pan, S.Y.Chail, C. Lee, S. E. Park, and W. I. Lee, *J. Phys. Chem. C*. **111**, 5582 (2007).
23. I. Jimenez, M. A. Centeno, R. Scotti, F. Morazzoni, J. Arbiol, A. Cornet, and J. R. Morante, *J. Mater. Chem.* **14**, 2412 (2004).
24. C. S. Rout, A. Govindaraj, and C. N. R. Rao, *J. Mater. Chem.* **16**, 3936 (2006).
25. C. C. Li, Z. F. Du, L. M. Li, H. C. Yu, Q. Wan, and T. H. Wang, *Appl. Phys. Lett.* **91**, 032101 (2007).
26. M. S. Hwang, and C. Lee, *Mater. Sci. Eng. B-Adv.* **75**, 24 (2000).
27. J. F. Chang, H. H. Kuo, I. C. Leu, and M. H. Hon, *Sens. Actuators B* **84**, 258 (2002).
28. N. Barsan and U. Weimar, *J. Electroceram.* **7**, 143 (2001).
29. A. R. Raju and C. N. R. Rao, *Sensor. Actuat. B-Chem.* **3**, 305 (1991).
30. D. Patil, L. Patil, and P. Patil, *Sensor. Actuat. B-Chem.* **126**, 368 (2007).
31. S. Park, H. Ko, S. Kim, and C. Lee, *ACS Appl. Mater. Interfaces* **6**, 9595 (2014).
32. K. Jain, R. P. Pant, and S. T. Lakshmikumar, *Sensor. Actuat. B-Chem.* **113**, 823 (2006).
33. E. Salje, *J. Appl. Crystallogr.* **7**, 615 (1974).
34. D. Miller, S. Akbar, and P. Morris, *Sensor. Actuat. B-Chem.* **204**, 250 (2014).
35. A. O. Gulino, P. Dapporto, P. Rossi, and I. Fragalà, *Chem. Mater.* **15**, 3748 (2003).
36. L. Xing, S. Yuan, Z. Chen, Y. Chen, and X. Xue, *Nanotechnology* **22**, 1 (2011).
37. X. Xie, Y. Li, Z. Q. Liu, M. Haruta, and W. Shen, *Nature* **458**, 746 (2009).
38. A. K. Chakraborty, Z. Qi, S. Y.Chail, C. Lee, S. Y. Park, D. J. Jang, and W. I. Lee, *Appl. Catal. B-Environ.* **93**, 368 (2010).
39. M.-C. Shin, J. H. Kim, J.-S. Cha, B. K. Shin, and H. S. Lee, *Korean J. Met. Mater.* **51**, 57 (2013).